Dimerization of boron triiodide at high pressure

Yansun Yao (姚延荪),[1] Dennis D. Klug,[1] Roman Martoňák,[2] and Serguei Patchkovskii[1]
[1]*Steacie Institute for Molecular Sciences, National Research Council of Canada, Ottawa, K1A 0R6, Canada*
[2]*Department of Experimental Physics, Comenius University, Mlynská dolina F2, 842 48 Bratislava, Slovakia*
(Received 3 March 2011; revised manuscript received 26 April 2011; published 9 June 2011)

High-pressure phase transition of boron triiodide (BI_3) is investigated using first-principles methods, with the crystal structure of the high-pressure phase predicted. The structure is consistent with the information on this phase available from experiments. Significantly, the BI_3 molecules are predicted to form B_2I_6 dimers that are structurally analogous to the D_{2h} diborane molecules. Dimerization of BI_3 molecules yields a notable volume drop that triggers a first-order phase transition. Using the predicted structure, the calculated equation of state, phase transition pressure, and the metallization transition pressure are in an excellent agreement with the experimental measurements. Dimerization in crystalline BI_3 provides insight for the understanding of covalently bound boron halide dimers, which were previously unknown.

DOI: 10.1103/PhysRevB.83.214105 PACS number(s): 64.70.kt, 62.50.−p, 61.50.Ks, 71.30.+h

I. INTRODUCTION

A remarkable feature of crystallography at high pressure is the existence of a rich diversity of crystal structures that are not accessible at ambient conditions. The driving force for the formation of these structures is the change in chemical bonding induced by high pressure. Upon compression, the pV work in solids increases and progressively modifies the Gibbs free energy. At sufficient compression, the pV work approaches typical bonding energies, distorting the existing chemical bonds and leads to new bonding. In molecular solids, donor-acceptor multicenter bonds become more common at high pressure, taking advantage of the extra orbitals made accessible by the increased coordination. The modified bonding environment tends to drive the molecular solids toward polymerization, eventually transforming the solids into nonmolecular forms. An important example of this tendency is given by the high-pressure phase transitions of N_2. Despite possessing very strong triple bonds in the molecular phase, N_2 is known to form a polymeric phase at high pressure, the so-called *cubic gauche* phase, constructed purely from single N-N bonds.[1,2] The molecular identity of N_2 is completely lost in this phase. In the present study, we report a theoretical investigation on the high-pressure phase transition of solid boron triiodide (BI_3) that follows very similar principles.

Under ambient conditions, BI_3 crystallizes into a molecular solid with a hexagonal unit cell. Each BI_3 molecule in the molecular solid possesses D_{3h} symmetry, which is identical to the molecular symmetry of BI_3 in the gas phase. Two BI_3 molecules are centrosymmetrically placed in the unit cell and lie on the basal planes at $z = 1/4$ and $4/3$, respectively. This arrangement yields the $P6_3/m$ (C_{6h}^2) space group for the BI_3 solid.[3] In a recent experiment, Hamaya *et al*. reported a high-pressure phase of BI_3 that forms above 6.2 GPa.[4] This high-pressure phase has extraordinary electronic properties that include the metallization at ∼23 GPa and a superconducting transition at ∼27 GPa. A detailed study of this high-pressure phase, however, is hindered by incomplete knowledge of the crystal structure. The x-ray diffraction patterns reveal that I atoms in this high-pressure phase form a face centered cubic (fcc) framework but the position of B atoms cannot be determined due to their low x-ray scattering cross sections. In the present study, we predict the likely structure for this high-pressure phase from first principles. The predicted structure is dynamically reachable on the free-energy surface and is consistent with all available experimental data. Significantly, the predicted structure is still a molecular solid, which is constructed from B_2I_6 dimers. The B_2I_6 dimer is structurally analogous to a diborane molecule[5] (B_2H_6) and has a distorted D_{2h} symmetry. The present prediction suggests that other heavy boron halides can also undergo dimerization, with the help of pressure. Until now, no covalently bound dimers have been known for trivalent boron halides. Although BF_3 is known to form weakly bound dimers in a cryogenic matrix, this structure arises primarily due to dispersive interactions between chemically intact BF_3 moieties.[6]

II. COMPUTATIONAL DETAILS

Structural optimizations, enthalpies, electronic band gaps, and vibrational densities of states (vDOS) presented in this study were calculated using a first-principles implementation of density-functional theory (DFT).[7] The vDOS were calculated using the ABINIT program[8] and Troullier-Martins pseudopotentials[9] with an energy cutoff of 40 Hartree, along with a $2 \times 2 \times 2$ q-point and an $8 \times 8 \times 8$ k-point mesh. Other calculations were performed using the Vienna *ab initio* simulation (VASP) program[10] and projector-augmented plane-wave (PAW) potentials[11] with an energy cutoff of 500 eV. The B and I potentials have $2s^2 2p^1$ and $5s^2 5p^5$ as valence states, respectively, employing the Perdew-Burke-Ernzerhof (PBE) exchange-correlation functional.[12] The Ceperley-Alder (CA) exchange-correlation functional[13] has also been employed to investigate the differences between local-density and generalized-gradient approximations (LDA and GGA). An $8 \times 8 \times 8$ k-point mesh was used in the structural optimizations and enthalpy calculations, while a denser $32 \times 32 \times 32$ k-point mesh was used in the electronic band-gap calculations. The metadynamics method[14,15] for the study of reconstructive phase transitions was employed and combined with the VASP program, which uses same parameters as described above. The supercells employed in the metadynamics calculations contained 8 BI_3 molecules and used a $2 \times 1 \times 1$ k-point mesh.

III. RESULTS AND DISCUSSION

A. Crystal structure of BI_3 at high pressure: Analysis

A review of the experimental data[4] indicates that several key observations can be made for the structure of the high-pressure phase of BI_3. The x-ray diffraction patterns show that the I atoms in this phase form an fcc framework, but no positional information can be extracted for the B atoms. Most likely, however, B atoms occupy the interstitial sites in the fcc lattice and may prefer tetrahedral sites over octahedral sites since occupation of the former yields stronger B-I bonds. Boron in BI_3 is three-coordinated (D_{3h}) at low pressure, therefore occupying a tetrahedral site (four-coordinated) requires formation of an additional covalent bond to the nearest molecule. This requires less energy than occupying an octahedral site (six-coordinated) and creating three additional bonds. Since boron has no available *d* orbitals for bonding, four-coordinated boron is commonplace in this element's chemistry while no 6-coordinated boron compounds are known.[16] Since there are more available tetrahedral sites than B atoms, one needs to determine the occupancy pattern of these sites. Experiments indicate that the high-pressure phase of BI_3 reverts to the $P6_3/m$ phase on releasing the pressure. Therefore, the high-pressure phase is likely ordered and structurally related to the $P6_3/m$ phase. The moderate pV work (at ~6.2 GPa) is not sufficient to dissociate the BI_3 molecules and transport B atoms to arbitrary tetrahedral sites. The occupancy pattern of the tetrahedral sites, therefore, is not random, yet the resulting high-pressure structure has to be dynamically reachable on the free-energy surface, i.e., it should not be blocked by energy barriers much in excess of kT.

Boron is well known to form B-B bonds in some of its compounds, e.g., in borides. Under high pressure, elemental boron is also shown to form B_2 pairs in a recent discovered γ-B_{28} phase.[17,18] In the high-pressure phase of BI_3, however, formation of B-B bonds is unlikely because the shortest possible B-B contact distance ($a_{fcc}/2$, a_{fcc} is the lattice constant) is always longer than the shortest B-I contact distance (~0.433 a_{fcc}), which contradicts the fact that B-B bonds are shorter than the B-I bonds. To form B_2 pairs between adjacent tetrahedral sites (by B-B σ bonds), the B atoms have to leave interstitial sites and this would inevitably destroy the fcc lattice, which does not conform to the experimental observations.

B. Determination of the crystal structure of BI_3 at high pressure

The above reasoning provides the starting point for numerical determination of the high-pressure phase. The calculations started with fcc supercells ($3 \times 1 \times 1$) constructed from 12 I atoms, and then adding 4 B atoms into each combination of four interstitial sites (both tetrahedral and octahedral). The fully relaxed structures show that, in general, the configurations with all B atoms in tetrahedral sites have the lowest enthalpies. This confirms the suggestion that in this high-pressure BI_3 structure, the tetrahedral sites are preferred over the octahedral sites. The octahedral sites have higher coordination, and therefore require greater pressures to be reached. We therefore only consider the BI_3 configurations with all B atoms located in tetrahedral sites. In a fcc supercell with $3n$ I atoms, each irreducible occupation of n tetrahedral sites represents a candidate BI_3 configuration. Candidate configurations were constructed from all possible occupations of a $3 \times 1 \times 1$ fcc supercell and from selected occupations of $3 \times 2 \times 1$ and $3 \times 2 \times 2$ fcc supercells. The constructed configurations were then fully relaxed to energy minima. Two structural constraints were applied to eliminate unreasonable configurations. (i) Each I atom is bonded to at least one B atom—this requires at least one of its nearest tetrahedral sites being occupied. (ii) Since the isolated BI_4 tetrahedron is not stable, it has to be bonded to other tetrahedrons and this requires at least one I atom in the tetrahedron having two of its nearest tetrahedral sites occupied. This structural construction scheme is efficient for the searching of the lowest energy phases of BI_3, but it is limited by the size of supercell employed. The number of possible BI_3 configurations increase exponentially with respect to the supercell size, making an extensive structural search impossible. We therefore cannot rule out the possibility that thermodynamically stable BI_3 phases with larger unit cells may exist.

Constructed high-pressure BI_3 structures are separated in three groups by their bonding patterns, with a representative structure from each group shown in Figs. 1(b) to 1(d) and compared with the $P6_3/m$ structure [Fig. 1(a)]. The first group, which contains most candidate structures, is characterized by infinite polymeric chains, with alternating B and I atoms [Fig. 1(d)]. The second group includes the structures formed

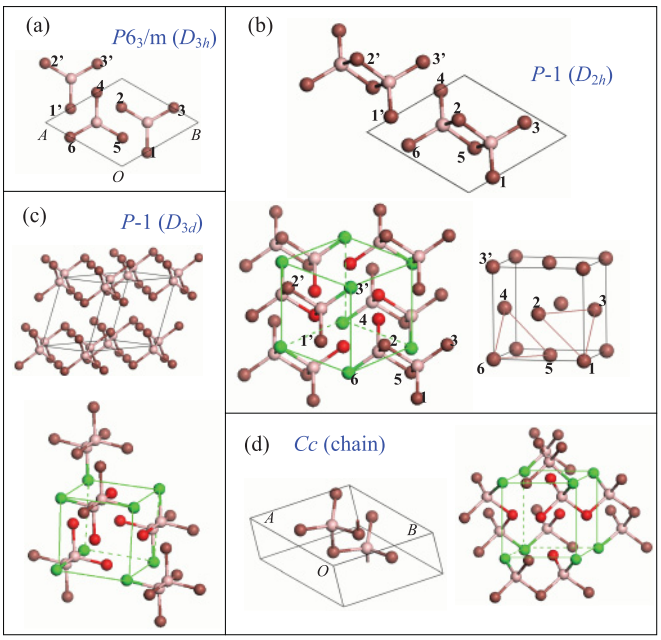

FIG. 1. (Color online) (a) The $P6_3/m$ structure in hexagonal unit cell. The BI_3 molecule with I(1), I(2), and I(3) atoms is located in the basal plane at $z = 1/4$, while the one with I(4), I(5), and I(6) atoms located at $z = 3/4$. The additional molecule with I(1′), I(2′), and I(3′) atoms is from the neighboring unit cell. Proposed high-pressure structures of BI_3 constructed from (b) D_{2h} dimers, (c) D_{3d} dimers, and (d) infinite polymeric chains of alternating B and I atoms. Indices of I atoms are provided in the D_{2h} dimer structure to demonstrate its structural relation with the $P6_3/m$ structure. The fcc unit cell is marked out by thin lines in all three structures with the face center I atoms highlighted by red (dark) color.

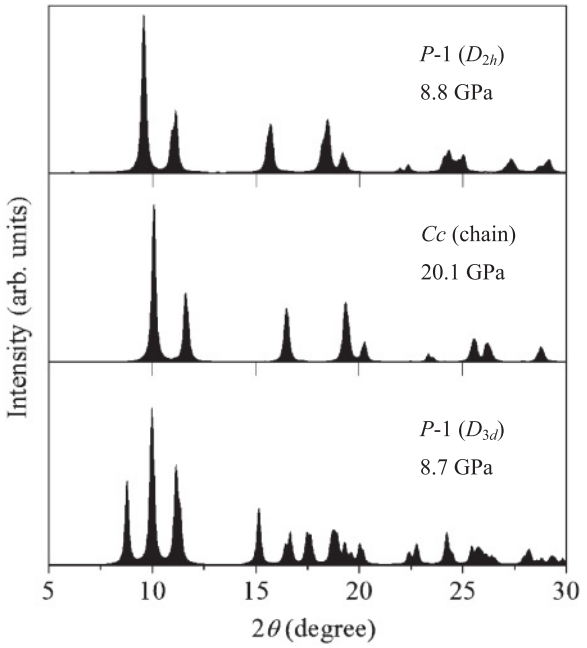

FIG. 2. Calculated x-ray diffraction patterns for candidate structures of high-pressure phases of BI_3 (x-ray wavelength = 0.5 Å).

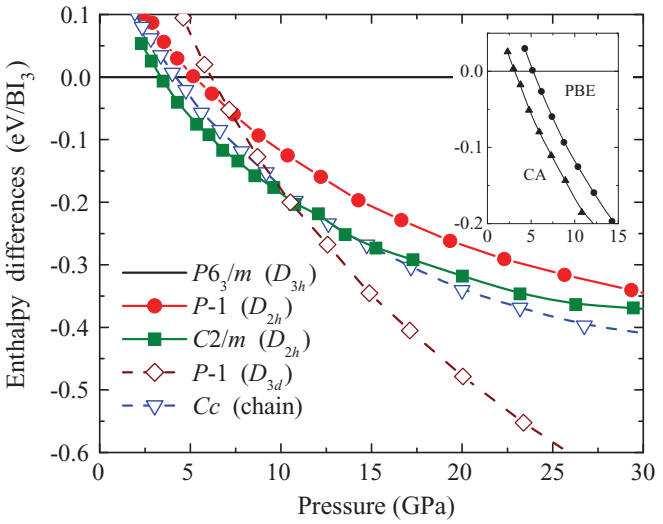

FIG. 3. (Color online) Calculated pressure dependence of enthalpies for selected high-pressure BI_3 structures relative to the $P6_3/m$ structure. The PBE exchange-correlation functional was employed in the calculations. Inset shows the differences between the PBE and CA exchange-correlation functionals, illustrated by the calculated enthalpies of the P-1 (D_{2h}) structure.

by molecular B_2I_6 dimers that are isostructural with the D_{2h} diborane molecule [Fig. 1(b)]. The third group contains structures formed by a different type of dimers that are isostructural with the D_{3d} ethane molecule [Fig. 1(c)]. Calculated x-ray diffraction patterns (Fig. 2) shows that, while both chain and D_{2h} dimer structures keep a basic fcc lattice (with minor distortions), the D_{3d} dimer structure deviates significantly from fcc. The D_{3d} dimerization is provided by formation of B-B σ bonds. At 8.7 GPa, the calculated B-B bond length in the D_{3d} dimer structure is about 1.66 Å, much shorter than the calculated B-I bond lengths ranging from 2.21 to 2.23 Å. The I-B-I and I-B-B bond angles in the D_{3d} dimer deviate substantially (up to 3°) from the ideal tetrahedral angle. These distortions break the T_d symmetry for boron sites and therefore destroy the fcc lattice (see Sec. III A). Electronic structure of the ethanelike B_2I_6 is chemically quite fascinating. Forming the two-center two-electron chemical bond between two B atoms requires "borrowing" two electrons from iodine lone pairs. As the result, B atoms acquire a formal -1 charge in the D_{3d} dimer, with I atoms carrying the compensating positive charge. Two possibilities exist for the source orbital of the B-B bonding electrons. If the electrons are extracted from a spatially nondegenerate linear combination of the lone pairs (A_{2g} irreducible representation in the D_{3d} point group), the resulting dimer retains D_{3d} symmetry in the gas phase. This structure is 1.32 eV less stable than the D_{2h} dimer in the gas phase. It is not expected to be significantly stabilized by nearest-neighbor electrostatic interactions in the solid state. The second possibility is to "borrow" the electrons from a spatially degenerate orbital (e.g., at the D_{3d} geometry). Although this possibility is less energetically favorable at D_{3d} geometry, the resulting electronic state undergoes a Jahn-Teller distortion. The resulting C_{2h} structure is stabilized by partial I-I bonds, formed between two pairs of neighboring electron deficient I atoms. The resulting gas-phase total energies of the D_{3d} and C_{2h} structures are nearly identical (less than 0.3 eV per dimer difference). Furthermore, one of the I atoms on each end of the molecule acquires an excess of electron density, so significant stabilizing electrostatic interactions are expected in the solid phase. Thus, the D_{3d} ethanelike high-pressure phase is best interpreted as a molecular solid of Jahn-Teller distorted C_{2h} B_2I_6 dimers. Significantly, formation of both locally stable ethanelike dimer structures correlates to an electronically excited state of the infinitely separated monomers. Such "thermally forbidden" reactions are typically associated with high activation barriers. In the solid state, they would be expected to proceed through a zero-band-gap intermediate.

The D_{2h} dimer and chain structures are close in enthalpies and become more stable than the $P6_3/m$ phase at a similar pressure ranging from 3.7 to 6.3 GPa (Fig. 3). This agrees very well with the experimental measurement of 6.2 GPa. A D_{2h} dimer structure with $C2/m$ space group is the lowest enthalpy configuration up to ~10.3 GPa, at which point it is superseded by a D_{3d} dimer structure with P-1 space group. Another D_{2h} dimer structure, which has the P-1 space group that represents a different packing pattern for the dimers, has higher enthalpies than the $C2/m$ structure. The chainlike structure with Cc space group has very close enthalpy to the $C2/m$ structure and becomes more stable than the latter at above 10.7 GPa. The D_{3d} dimer structure is, however, not compatible with the x-ray diffraction measurements although it has notably lower enthalpy than other candidate structures at higher pressures. The enthalpies calculated using CA exchange-correlation functional reveal the same stability order for the candidate structures, while the predicted transition pressures are lowered by ~3 GPa (Fig. 3, inset).

To identify the actual BI_3 structure formed at high pressure, it is helpful to characterize chemical bonding in the candidate structures and rationalize transformation pathways from which they evolved from the parent $P6_3/m$ structure. Structural

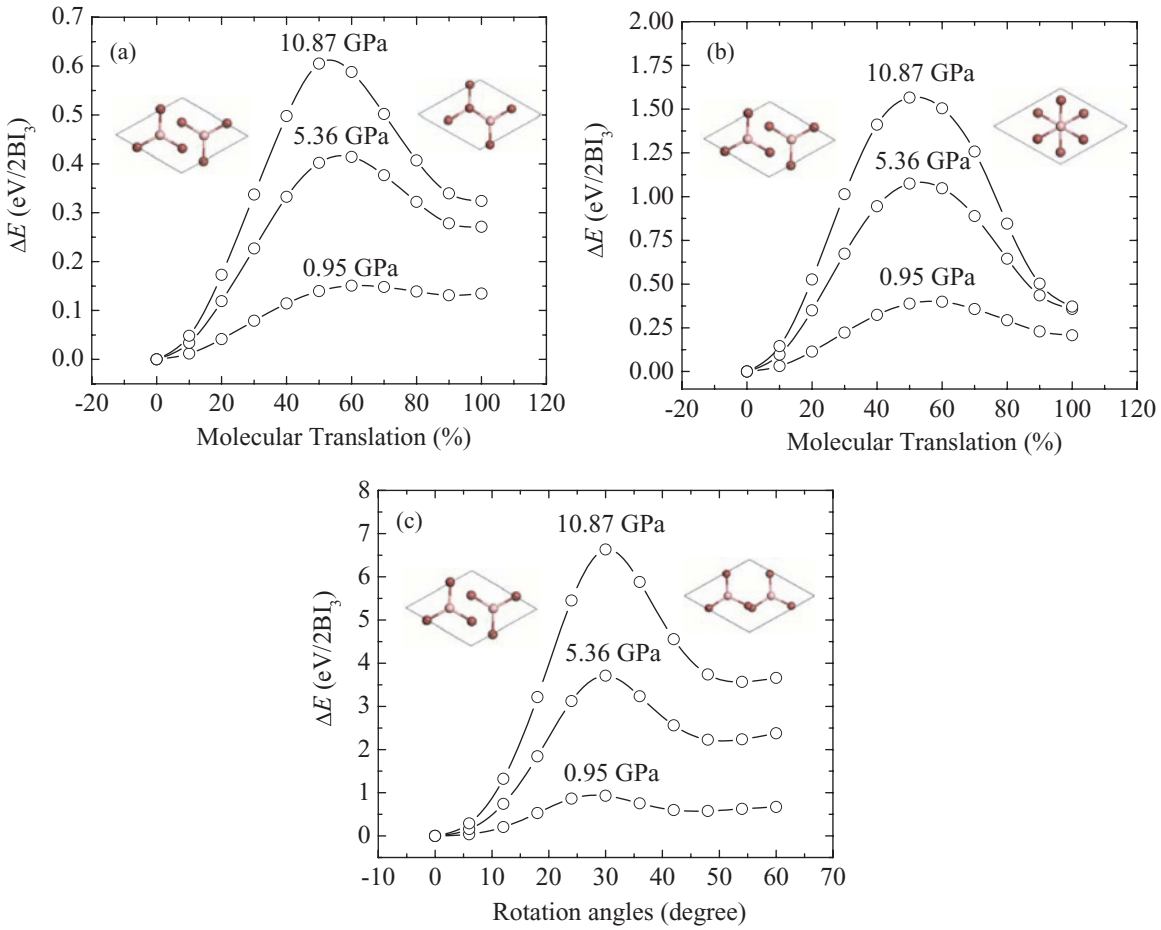

FIG. 4. (Color online) Calculated energy changes in the $P6_3/m$ unit cell during three representative molecular movements. In (a) and (b) for molecular translations, two BI_3 molecules move toward each other until the B atom from one molecule aligns with (a) the closest I atom or (b) the B atom from the other molecule along the z axis. In (c) for a molecular rotation path, one BI_3 molecule rotates by 60° with respect to the B atom while the other molecule is fixed. Insets show the top view of the $P6_3/m$ structure before and after the molecular movements.

transformation from the $P6_3/m$ to D_{2h} dimer structures involves mainly localized molecular translations [Fig. 1(b)]. Two adjacent BI_3 molecules move toward each other and form a B_2I_6 dimer by creating two new B-I bonds, which connect I(2) and I(5) atoms to the other BI_3 molecule. The new bonds are nearly perpendicular to the original BI_3 planes and pull the B atoms off the plane to become tetrahedrally coordinated. In the P-1 structure [Fig. 1(b)], I(1), I(2), and I(3') atoms become equally spaced and align in a face diagonal of the fcc lattice. For comparison, in the $P6_3/m$ structure, these three atoms form an angle ~170.4° near ambient conditions. The line I(6)-I(1) becomes an fcc lattice edge and obviously forms a 45° angle with the I(2) atom. This angle is ~58.4° in the $P6_3/m$ near ambient conditions. The D_{2h} dimerization does not involve strong I-I interactions and therefore proceeds with moderate compression. Figure 4(a) shows the estimated energy changes on the molecular translations for D_{2h} dimerization in the $P6_3/m$ unit cell, in which two BI_3 molecules move simultaneously until I(2) and I(5) atoms align along the z axis with the B atom from the other molecule. The energy barriers (upper-bound estimates) associated with these molecular translations are low. At 5.36 GPa, which is close to the phase transition pressure, the energy barrier is only ~0.4 eV/unit cell, less than half of the energy barrier for D_{3d} dimerization [Fig. 4(b)]. Pathways to formation of chain structures [Fig. 1(d)] differ strikingly from that of the dimer structures. In a polymeric chain each BI_3 molecule is bonded with two distinct BI_3 neighbors, and therefore, the phase transition requires molecular rotations in addition to translations. For example, to form the Cc structure [Fig. 1(d)] from the $P6_3/m$ structure, one molecule in the unit cell needs to rotate 60° and bond with two neighbors from two adjacent basal planes. Due to additional molecular rotations, polymeric chain formation would be energetically less favorable when compared to dimerization. Molecular rotations in the $P6_3/m$ structure are therefore hindered in the close proximity of neighboring molecules, and the BI_3 monomers only undergo librational vibrations.[19] On increasing pressure, the strengthened nonbonded I-I interactions would make the molecular rotations even more difficult. Figure 4(c) shows the estimated rotational barriers (upper-bound estimates) in the $P6_3/m$ unit cell, in which one BI_3 molecule continuously rotates 60° while the other molecule is fixed. The rotational barrier is about one order of magnitude larger than the translational barrier for D_{2h} dimerization. At 5.36 GPa, the rotational

barrier is 3.71 eV/unit cell, precluding the transformation altogether.

A low energy barrier associated with the D_{2h} dimerization makes it the most likely motif for high-pressure phase of BI_3. To examine this hypothesis, metadynamics calculations were employed to directly simulate the phase transition. Metadynamics calculations were performed at 10, 20, and 30 GPa, with a 32 atom (8 BI_3 molecules) supercell. The supercell was constructed by converting the $P6_3/m$ unit cell to an orthorhombic cell, applying the basic vectors (1, 1, 0), (-1, 1, 0), (0, 0, 1) on the hexagonal lattice vectors and doubling the resulting cell along the c axis. The metadynamics algorithm is an efficient method to simulate reconstructive phase transitions that is able to search for low-energy pathways leading from the initial free-energy well to neighboring minima without excessively overpressurizing the system. Successful applications of the method include several examples of high-pressure phase transitions[20–24] (see, e.g., SiO_2, Si, CO_2, C, and Ca). Room-temperature metadynamics simulations were performed employing Gaussian width and height parameters of 15 (kbar Å^3)$^{1/2}$ and 225 kbar Å^3 (140.4 meV), respectively, and starting from the initial $P6_3/m$ structure. The metadynamics algorithm used in the present study as well as guidelines how to choose the Gaussian size have been summarized recently in Refs. 25 and 26. Figure 5(a) shows the enthalpy evolution in the metadynamics simulation at 20 GPa. There is an initial restructuring of the $P6_3/m$ supercell occurring almost immediately after initial equilibration at 300 K employing an NVT ensemble. A prominent enthalpy drop starts at metastep 23, corresponding to the onset of the formation of a new phase. The phase transition proceeds without passing any stable intermediate phase and settles into a new structure with D_{2h} dimers; the simulation concurs nicely with the qualitative analysis. Structural analysis shows that this dimer structure coincides with the P-1 structure shown in Fig. 1(b). Figure 5(b) shows the detailed structural evolution from the $P6_3/m$ to P-1 structure in the metadynamics simulation. At the initial stage of transformation, a drop in enthalpy (metasteps 1 to 5) results from D_{2h} dimerization in alternate pairs of layers in the simulation cell, caused by relative displacements of adjacent BI_3 layers. Dimerization then continues to spread throughout the entire simulation cell and the structural evolution after metastep 23 results in the P-1 structure constructed from layers of D_{2h} dimers. No molecular rotations occur in the simulated phase transition. The I atoms form a fcc lattice with one unit spanning over 3 B_2I_6 layers, and the B atoms occupy selected tetrahedral sites. Metadynamics simulations performed at 10 and 30 GPa predicted the same P-1 structure.

According to the enthalpy calculations, the suggested P-1 structure becomes more stable than the $P6_3/m$ structure near 5.2 GPa (Fig. 3). This is in good agreement with the measured high-pressure phase transition that starts at 6.2 GPa (reverse transition occurs at 5.0 GPa). The differences between calculated and measured transition pressures could be attributed to many factors, e.g., absence of kinetic effects in the calculations and limitations in pseudopotential-DFT approaches. The $P6_3/m \rightarrow P$-1 phase transition is also accessible on the free-energy surface as shown by the metadynamics calculations. The P-1 space group corresponds to a particular packing pattern for the D_{2h} dimer layers, and by changing the

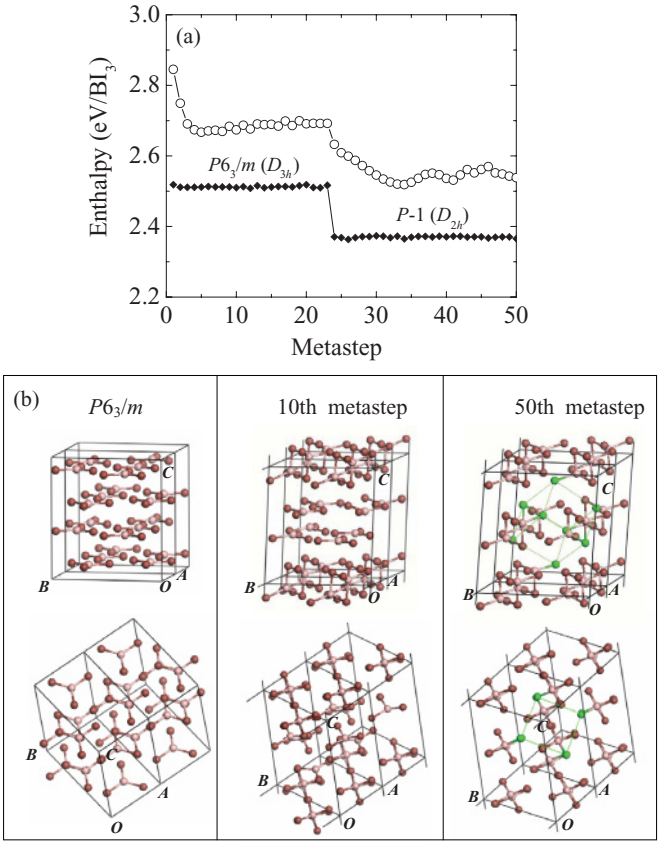

FIG. 5. (Color online) Metadynamics simulation at 20 GPa and 300 K, starting from the initial $P6_3/m$ structure. (a) Enthalpy evolution in the simulation (empty symbols) and enthalpies for configurations after structural optimizations (solid symbols). (b) Initial $P6_3/m$ structure and structures at metasteps 10 and 50. The fcc lattice formed after the phase transition is highlighted.

packing pattern, one can reach different crystal structures and some of them have lower enthalpies than the P-1 structure, for example, the $C2/m$ structure (Fig. 3). The formation of the P-1 structure is facilitated by a low energy barrier since it requires the least molecular translations. A comparison between the optimized supercells in the metadynamics simulation before and after the phase transition shows that the $P6_3/m$ to P-1 phase transition involves only local molecular translations [Figs. 6(a) and 6(b)]. Each pair of adjacent BI_3 layers move the shortest distance to form a dimer layer, and there are no additional movements between the dimer layers once they formed. The resulting packing pattern for the dimer layers in the P-1 structure is shown in Fig. 6(c). In contrast, formation of the $C2/m$ structure [Fig. 6(d)] requires an additional shearing between the dimer layers and this increases the height of the energy barriers. The actual dimerization mechanism is likely initiated by a nucleation step and associated with lower energy barriers. Theoretical suggestions for packing patterns are also subject to the limitation of the calculations (e.g., size of the simulation cell and length of simulation time). Thus, it is possible that the actual high-pressure phase of BI_3 may involve other packing patterns for the D_{2h} dimer layers than what is suggested here.

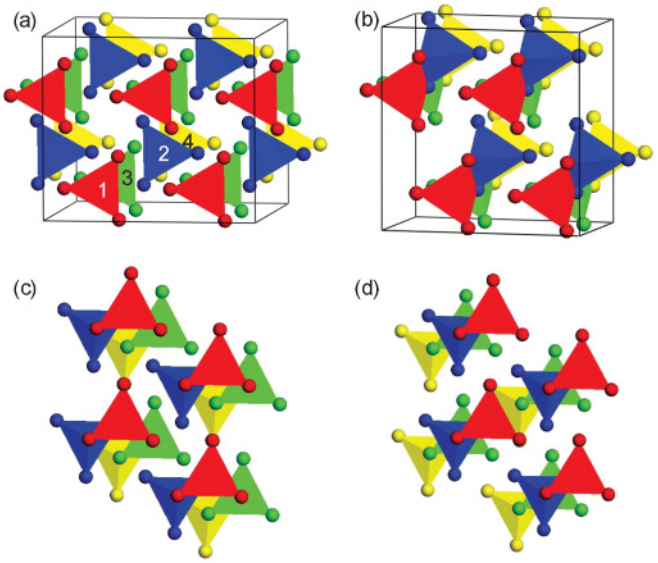

FIG. 6. (Color online) (a) Initial $P6_3/m$ supercell and (b) optimized P-1 supercell before and after the phase transition in the metadynamics simulation. The initial $P6_3/m$ supercell contains four layers of BI_3 monomers, with the identical layers 1 (red) and 3 (green) alternating with identical layers 2 (blue) and 4 (yellow). The BI_3 and B_2I_6 molecules are shown by polyhedrons. (c) P-1 and (d) $C2/m$ structures viewed along a threefold axis of the tetrahedrons, which is nearly perpendicular to the original basal planes. The two structures have different packing patterns for the dimer layers.

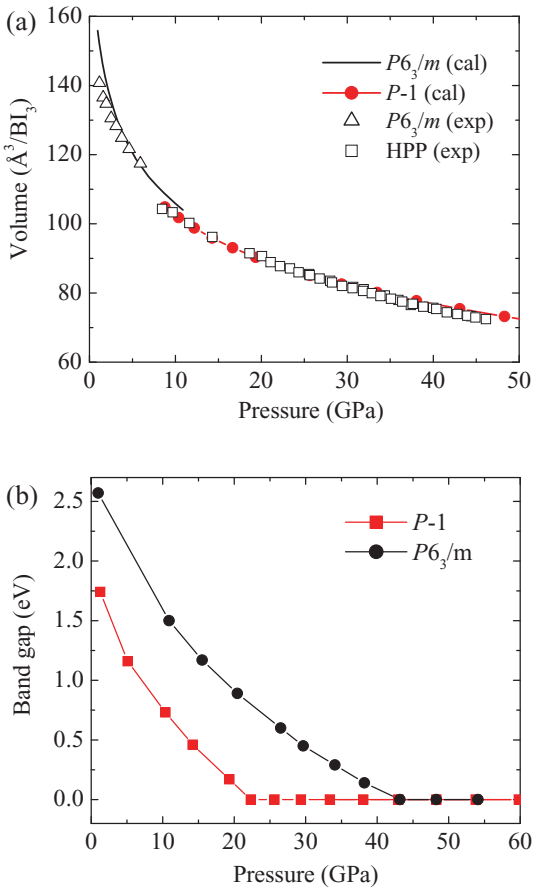

FIG. 7. (Color online) (a) Calculated pressure-volume curves (cal) for the $P6_3/m$ and predicted P-1 phases, compared with the measurements (exp) for the $P6_3/m$ and the high-pressure phases (HPP). The experimental data are from Ref. 4. (b) Calculated magnitudes of band gap as functions of pressure for the $P6_3/m$ and predicted P-1 phases.

C. Dimerization in BI_3 at high pressure

The predicted D_{2h} dimer is stabilized by a pair of equivalent B-I-B bonds through the bridging I atoms [Fig. 1(b)]. The electronic structure of this B_2I_6 dimer also shares some similarity with that of the Al_2Cl_6 dimer,[27] as the forming elements of these two dimers are in same group in the periodic table of elements. In the BI_3 monomer, three sp^2 hybrid orbitals of B atom form σ bonds with three equivalent terminal I atoms. This leaves an unhybridized p orbital of B atom formally unoccupied. This orbital is stabilized by π back-donation from the lone pairs of the halogen ligands. This interaction, which is not present in the isostructural D_{3h} BH_3, stabilizes the planar BI_3 monomer at ambient conditions. At high pressure, the intermolecular distances in the $P6_3/m$ structure decrease, and, at some point, the B coordination has to increase. For BI_3 monomers, increased B coordination (from 3 to 4) proceeds naturally by pyramidalization associated with a change to the sp^3 hybridization. In a D_{2h} dimer, the empty sp^3 hybrid orbital on one BI_3 monomer attracts a lone electron pair on the nearest terminal I atom from the other monomer and forms a donor-acceptor B-I bond that extends the existing covalent B-I bond to form a B-I-B bridge. Two identical B-I-B bridges are formed in each D_{2h} dimer [Fig. 1(b)]. The overall bonding strength of the B-I-B bridges is weaker than that of the B-I terminal bonds. In each bridge, the donor-acceptor B-I bond is nearly perpendicular to the original BI_3 planes and holds the two planes together [Fig. 5(b)]. This bonding is a little weaker than the covalent bonding within the planes and acquires a slight polarity toward the I atom. This bonding feature is revealed by the calculated B-I distances. For example, in the P-1 structure near 5 GPa, the calculated B-I distances for donor-acceptor and covalent components in the B-I-B bridge are 2.36 Å and 2.29 Å, respectively, while the terminal B-I bonds have a shorter length of 2.16 Å. In a crystalline solid, dimers are subject to structural distortions resulting from nonbonded interactions with their neighbors. In the P-1 structure, D_{2h} dimers reduce their symmetry to C_i, a subgroup of C_{2h} symmetry. In the ideal fcc lattice, boron sites must exhibit local T_d symmetry. Formation of the C_i symmetric B_2I_6 dimers lowers this ideal site symmetry, causing small distortion from the perfect fcc crystal, which has been also noted in the experiment. A necessary consequence of dimerization is the reduction in the molar volume. This accounts for the reported volume drop in the high-pressure phase transition of BI_3. Using the predicted P-1 structure as the candidate, the pressure-volume (P-V) curve for the high-pressure phase has been calculated, and the results show excellent agreement with the measured data[4] [Fig. 7(a)]. The calculated P-V curve for the $P6_3/m$ structure also agrees well with the experiment, except below 3 GPa it starts to deviate from experiment which is most likely due to the well-known deficiency of DFT in treating dispersive interactions.

D. Reconciling the prediction and experiments

Additional comments can be made to reconcile the predicted P-1 structure with the observations on the high-pressure phase of BI_3 made by Hamaya *et al*. based on their experimental data.[4] First, it was proposed that at the transition point, the stacking periodicity of the BI_3 layers in the $P6_3/m$ structure exhibits an abrupt drop, whereas the periodicity within the layers decreases continuously. It was then suggested that this led to a breakdown of the BI_3 molecules resulting in a monatomic phase with B atoms possibly occupying tetrahedral sites randomly in the fcc lattice formed by the I atoms. The possibility of a structure consisting of periodic dimeric units was not considered. Clearly, the drop in the stacking periodicity is consistent with the formation of donor-acceptor B-I bonds between two adjacent BI_3 layers [Fig. 5(b)], which are nearly perpendicular to the layers and decrease the interlayer distances. Within the layers, in contrast, the modification of the bonding is small and therefore does not abruptly destroy the periodicity. Hamaya *et al*. also suggested that at the phase transition point, the intramolecular distance, r_{21} [distance between I(1) and I(2) atoms, Fig. 1(a)] should reach the intermolecular distance, $r_{23'}$. This can be seen in the P-1 structure, where the I(1), I(2), and I(3′) atoms align as a face diagonal of the fcc lattice, and, therefore, both r_{21} and $r_{23'}$ correspond to half of the face diagonal [Fig. 1(b)]. The original basal planes become (111) planes of the fcc lattice. Hamaya *et al*. further commented that the angle I(1′)-I(2)-I(3′) in the $P6_3/m$ structure should increase with pressure and approach 60°, but the phase transition would occur before it reaches 60°. In the P-1 structure [Fig. 1(b)], the I(3′) atom is a corner atom in the fcc lattice, while I(1′) and I(2) atoms are two closest face centers. If the fcc lattice is not distorted, the angle I(1′)-I(2)-I(3′) should be 60°. The smaller I(1′)-I(2)-I(3′) angle at the transition point, i.e., ∼58°, indicates that the high-pressure phase should deviate slightly from an ideal fcc lattice, which is consistent with the distortions of the D_{2h} dimers in the P-1 structure.

E. Metallization and stability for BI_3 at high pressure

In the experiment, BI_3 is found to become metallic at ∼23 GPa and exhibits weak superconductivity above ∼27 GPa.[4] Using the P-1 structure as the candidate, the calculated pressure for the band-gap closure in BI_3 is about 22.3 GPa [Fig. 7(b)], showing excellent agreement with the experiment. In contrast, the calculated pressure for band-gap closure in the $P6_3/m$ structure is much higher, i.e., 43.2 GPa [Fig. 7(b)]. The significantly lower pressure for metallization in the P-1 structure demonstrates the important role that dimer formation plays in the metallization. The metallization procedure of BI_3 is directly related to the enhancement of intermolecular interactions. The molecular orbitals of BI_3 monomers are delocalized at high pressure and therefore overlap more strongly with each other. This tends to lower energy levels of the bonding states with respect to that of the antibonding states and therefore increases the bandwidth and decreases the energy gap.[28] Formation of the extended B-I-B bridging bonds on dimerization strengthens the orbital overlaps and accelerates the metallization. It is interesting to note that elemental iodine becomes metallic at about 16 GPa (Ref. 29), notably lower than the pressure for metallization in BI_3. The presence of boron atoms therefore suppresses the conductivity of the iodine framework in BI_3. This is not surprising since elemental boron requires more than 10 times higher pressure than elemental iodine, i.e., above 160 GPa, to reach a metallic state.[30,31] A previous theoretical calculation[17] suggested that the charge transfer between the B_2 pairs and icosahedral B_{12} clusters hinders the metallization in the high-pressure γ-B_{28} phase, and metallization in elemental boron could eventually be reached by the breakup of B_{12} clusters at much greater pressure.[17,31]

At the onset of the superconducting transition, the measured superconducting critical temperature (T_c) is 0.5 K. It further increases up to 2 K by further compression. The present prediction of the crystal structure will enable a theoretical investigation on the superconductivity of BI_3 to proceed, presumably using the electron-phonon interactions as included in the Eliashberg theory[32] and assuming the BI_3 compound is a BCS-type superconductor.[33] The stability of the D_{2h} dimer motif at high pressure was established from phonon calculations [Figs. 8(a) and 8(b)]. The absence of imaginary vibrational frequencies in both P-1 and $C2/m$ structures confirms that these two D_{2h} dimer structures are stable.

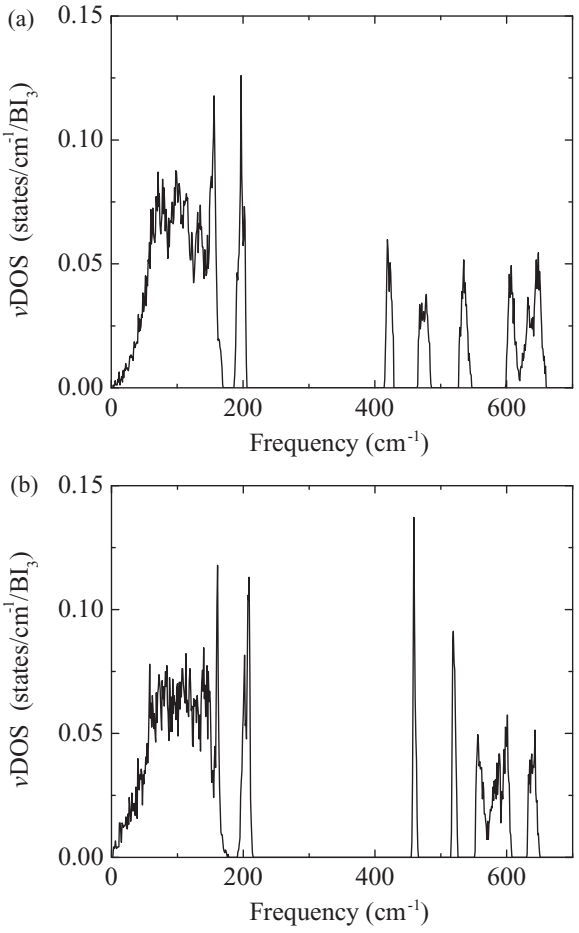

FIG. 8. Vibrational density of states (νDOS) for the (a) P-1 and (b) $C2/m$ phase calculated near 20 GPa. The two structures differ only in the packing patterns for the D_{2h} dimer layers [see Figs. 6(c) and 6(d)].

Both vibrational DOS show a large fraction of vibrations in the low-frequency region that originate mainly from heavy I atoms. Qualitatively, the low-frequency vibrations may help to promote phonon-mediated superconductivity, but the low charge-carrier concentration (delocalized electrons from dimers) would hinder the electron-phonon couplings, and a low T_c appears as a result of competition between the two mechanisms. Nevertheless, the appearance of superconductivity in BI_3 at high pressure may not be surprising since the elemental and molecular components, B and I_2, are both superconducting at high pressure.[30,34]

IV. SUMMARY

In the present study, we used theoretical methods to investigate a recently reported high-pressure phase transition in BI_3 and predicted the crystal structure for the high-pressure phase. In the predicted structure, each pair of two closest BI_3 molecules forms a B_2I_6 dimer that is structurally analogous to the diborane dimer. The B_2I_6 dimer has a C_i symmetry and is only slightly distorted from the ideal D_{2h} symmetry. In the extended lattice, the I atoms of B_2I_6 dimers form a basic fcc lattice, which also deviates from the ideal symmetry due to the distortions in the dimers. The B atoms are located in selected tetrahedral sites of the fcc lattice of I atoms. The structural features of the predicted structure are consistent with the available measurements on the high-pressure phase of BI_3. Dimerization of BI_3 molecules also explains the observed volume drop accompanying the phase transition. The calculated equation of state and metallization pressure using the predicted dimer structure agree very well with the experimental data. It is suggested therefore that the high pressure phase of BI_3 may be better described as one consisting of ordered dimeric components than a structure characterized as monatomic with randomly located boron atoms at tetrahedral sites in a fcc lattice of iodine atoms. To date, no covalently bound trivalent boron halides have been known to exist. The predicted dimerization in BI_3 under high pressure in this study suggests a possible route to form boron halide dimers with the heavy halogen atoms.

ACKNOWLEDGMENTS

Y.Y. is grateful to Professor Roald Hoffmann for valuable discussions and suggestions. R.M. has been supported by the Slovak Research and Development Agency under Contracts No. APVV-0442-07 and No. VVCE-0058-07 and by the project implementation 26240120012 within the Research & Development Operational Programme funded by the ERDF.

[1] C. Mailhiot, L. H. Yang, and A. K. McMahan, Phys. Rev. B **46**, 14419 (1992).
[2] M. I. Eremets, A. G. Gavriliuk, I. A. Trojan, D. A. Dzivenko, and R. Boehler, Nat. Mater. **3**, 558 (2004).
[3] B. Albert and K. Schmitt, Z. Anorg. Allg. Chem. **627**, 809 (2001).
[4] N. Hamaya, M. Ishizuka, S. Onoda, J. Guishan, A. Ohmura, and K. Shimizu, Phys. Rev. B **82**, 094506 (2010).
[5] R. C. Lord and E. Nielsen, J. Chem. Phys. **19**, 1 (1951).
[6] J. M. Bassler, P. L. Timms, and J. L. Margrave, J. Chem. Phys. **45**, 2704 (1966).
[7] W. Kohn and L. J. Sham, Phys. Rev. **140**, A1133 (1965).
[8] X. Gonze, J. M. Beuken, R. Caracas, F. Detraux, M. Fuchs, G. M. Rignanese, L. Sindic, M. Verstraete, G. Zerah, F. Jollet, M. Torrent, A. Roy, M. Mikami, Ph. Ghosez, J.-Y. Raty, and D. C. Allan, Comput. Mater. Sci. **25**, 478 (2002).
[9] N. Troullier and J. L. Martins, Phys. Rev. B **43**, 1993 (1991).
[10] G. Kresse and J. Hafner, Phys. Rev. B **47**, 558 (1993).
[11] G. Kresse and D. Joubert, Phys. Rev. B **59**, 1758 (1999).
[12] J. P. Perdew, K. Burke, and M. Ernzerhof, Phys. Rev. Lett. **77**, 3865 (1996).
[13] D. M. Ceperley and B. I. Alder, Phys. Rev. Lett. **45**, 566 (1980); parametrized by J. P. Perdew and A. Zunger, Phys. Rev. B **23**, 5048 (1981).
[14] R. Martoňák, A. Laio, and M. Parrinello, Phys. Rev. Lett. **90**, 075503 (2003).
[15] R. Martoňák, D. Donadio, A. R. Oganov, and M. Parrinello, Nat. Mater. **5**, 623 (2006).
[16] N. N. Greenwood and A. Earnshaw, *Chemistry of the Elements*, 2nd ed. (Butterworth-Heinemann, Oxford, UK, 1997).
[17] A. R. Oganov, J. Chen, C. Gatti, Y. Ma, Y. Ma, C. W. Glass, Z. Liu, T. Yu, O. O. Kurakevych, and V. L. Solozhenko, Nature **457**, 863 (2009).
[18] E. Yu. Zarechnaya, L. Dubrovinsky, N. Dubrovinskaia, Y. Filinchuk, D. Chernyshov, V. Dimitriev, N. Miyajima, A. El Goresy, H. F. Braun, S. Van Smaalen, I. Kantor, A. Kantor, V. Prakapenka, M. Hanfland, A. S. Mikhaylushkin, I. A. Abrikosov, and S. I. Simak, Phys. Rev. Lett. **102**, 185501 (2009).
[19] A. Anderson and J. Lauren Lettress, J. Raman Spectrosc. **33**, 173 (2002).
[20] D. Donadio, R. Martoňák, P. Raiteri, and M. Parrinello, Phys. Rev. Lett. **100**, 165502 (2008).
[21] J. Behler, R. Martoňák, D. Donadio, and M. Parrinello, Phys. Rev. Lett. **100**, 185501 (2008).
[22] J. Sun, D.D. Klug, and R. Martoňák, J. Chem. Phys. **130**, 194512 (2009).
[23] J. Sun, D.D. Klug, R. Martoňák, J.A. Montoya, M.S. Lee, S. Scandolo, and E. Tosatti, Proc. Natl. Acad. Sci. USA **106**, 6077 (2009).
[24] Y. Yao, D.D. Klug, J. Sun, and R. Martoňák, Phys. Rev. Lett. **103**, 055503 (2009).
[25] R. Martoňák, in *Modern Methods of Crystal Structure Prediction*, edited by A.R. Oganov (Wiley-VCH, Berlin, 2011).
[26] R. Martoňák, Eur. Phys. J. B **79**, 241 (2011).
[27] S. D. Williams, W. Harper, G. Mamantov, L. J. Tortorelli, and G. Shankle, J. Comput. Chem. **17**, 1696 (1996).
[28] R. Hoffmann, *Solids and Surfaces: A Chemist's View of Binding in Extended Structures* (VCH, New York, 1988).
[29] A. S. Balchan and H. G. Drickamer, J. Chem. Phys. **34**, 1948 (1961).
[30] M. I. Eremets, V. V. Struzkhin, H. Mao, and R. J. Hemley, Science **293**, 272 (2001).

[31]D. N. Sanz, P. Loubeyre, and M. Mezouar, Phys. Rev. Lett. **89**, 245501 (2002).

[32]G. M. Eliashberg, Zh. Eksp. Teor. Fiz. **38**, 966 (1960) [Sov. Phys. JETP **11**, 696 (1960)].

[33]J. Bardeen, L. N. Cooper, and J. R. Schrieffer, Phys. Rev. **108**, 1175 (1957) .

[34]K. Shimizu, N. Tamitani, N. Takeshita, M. Ishizuka, K. Amaya, and S. Endo, J. Phys. Soc. Jpn. **61**, 3853 (1992).